Mechanical Characterization of the Human Auricle for Earable Device Design

Y. Li[a], M.L. Bance[b], M.P.F. Sutcliffe[a]

[a] *Department of Engineering, University of Cambridge, CB2 1PZ, Cambridge, UK*
[b] *Department of Clinical Neurosciences, University of Cambridge, CB2 0XY, Cambridge, UK*

Abstract

The human auricle, despite its intricate anatomy and biomechanical significance, remains relatively under-studied in terms of its mechanical properties. This work aims to characterise the mechanical behaviour of human auricles and provide novel experimental and modelling tools to simulate this response, with a focus on informing the design of wearable ear devices, or 'earables'. A realistic phantom auricle model was constructed with the aim of providing an experimental tool for use in researching auricle mechanical properties. This tool proved its worth by being used to develop a methodology for testing the mechanical response of human auricles. A volunteer study was then conducted using this methodology to characterise the mechanical and structural behaviour of the human auricle. In static loading tests, the force required to bend human auricles was found to vary from 0.09 N to 0.15 N for an applied displacement equal to 25% of the auricle's width. In dynamic loading tests, the measured natural frequency of the human auricle ranged from 13 Hz to 27 Hz. Finally, a finite element computational model was developed to simulate the measured mechanical behaviour of the human auricle. The aim was to provide a computational tool to use alongside the experimental phantom tool to explore the mechanical response of human auricles in conjunction with earables. This model was validated by comparison with the measured human auricle data.

Keywords: Finite Element Analysis, Auricle, Pinna, Biomechanical properties

1. Introduction

'Earables' (Röddiger et al., 2022) are increasingly popular wearable devices which use the external ear, the auricle, as their primary support (He et al., 2015; Papapanagiotou et al., 2017). The ear's location near the brain allows earables to function as neural interfaces (Choudhury, 2021). With attached skin electrodes, earables can record neural signals such as electroencephalograms (EEG) (Debener et al., 2015). Earables signals can, however, be affected by the body's movement and vibrations, causing artefacts. Previous studies have mostly focused on functionality, considering electrode stretchability (Wu et al., 2021) and the signal-to-noise ratio of electrodes for EEG signals (Kappel et al., 2019). Another crucial limitation is the unstable contact between the electrodes and the skin (Goyal et al., 2022). This highlights the need for a comprehensive model of the auricle's mechanical behaviour to understand its interaction with earable devices during daily activities.

The first step in building an auricle mechanical model is to consider the geometry and material properties of the ear. Figure 1 illustrates the anatomy of the human auricle. The auricle is composed of the auricular cartilage and covering skin (Felfela, 2017). The stiffness of auricular cartilages was measured using compression testing on samples from different anatomical regions (Griffin et al., 2016). The reported average Young's modulus of auricular cartilage is 1.66 ± 0.63 MPa. The measured Young's modulus of the skin has a large variation, dependent on the test method used (Pawlaczyk et al., 2013). The typical Young's modulus of human skin measured with the suction method is between 0.05 MPa and 0.15 MPa (Hendriks et al., 2003).

Although the material properties of auricular tissues have been well studied, there are no studies focusing on the structural mechanics of the auricle. A common experimental approach in biomechanical studies is to use realistic phantom models to mimic the *in vivo* test environment. For example, such phantoms have been used for analysing in-ear device insertions (Benacchio et al., 2018). When modelling soft tissues, these phantom models are usually made of soft materials such as silicone gels, with 3D printing being a widely adopted part of the manufacturing process (Higgins et al., 2022).

Finite Element (FE) analysis is widely used in biomechanical studies as it allows the numerical simulation of the mechanical behaviour of parts with complex shapes and varying material properties (Brenner and Scott, 2008). Since ear mechanics are difficult to measure due to the complexity of living tissue, FE methods provide a great tool for studying the auricle structural mechanics. Models of the ear have so far focussed on the ear canal and middle ear, addressing sound propagation and hearing functionality (Areias et al., 2017) rather than considering the structural behaviour of the auricle.

This study aims to provide tools and characterisation data to allow assessment of the mechanical be-

haviour of the human auricle, especially as related to earable design and use. Three specific objectives contribute to this overall aim as illustrated in Figure 2: (i) development of a realistic physical phantom which can be used as a tool to explore mechanical aspects of auricle-earable interactions experimentally; (ii) collection of experimental data from volunteer subjects characterising the structural mechanical response of the human auricle; and (iii) development of a computational FE auricle model which can be used for numerical studies, for example to optimise earable design. As illustrated in Figure 2 these three objectives are interlinked, with the phantom demonstrating its utility by providing a way of developing the methodology for human auricle study, while the human auricle experiments provide data to validate the computational model.

The paper is structured into three sections presenting the methods and results from each of the objectives in turn. First the phantom development is presented and applied to development of a test methodology for mechanical characterisation. Then the human volunteer study is detailed. Finally the development of the FE model and a comparison with experimental results is presented. The paper finishes with a Discussion section and Conclusions.

2. Phantom model development and application in designing a mechanical test protocol

The aim of developing the realistic auricle phantom model is to provide a practical tool for testing the mechanical response of auricles, including earable interactions, through an *in vitro* test environment. This section first describes the development of the phantom itself and then demonstrates its application in developing a test methodology to apply to the human auricle testing programme of section 3.

2.1. Phantom design and manufacture

The model was constructed from two parts with different moduli to represent skin and cartilage. The 3D model of the auricle was derived from a medical image of a cadaveric ear sample provided by Hrncirik et al. (2022). This scanned model was processed and simplified using mesh editing software (Meshmixer 3.5; Autodesk, CA), as illustrated in Figure 3(a). The simplification resulted in a model with increased thickness compared to the original auricle, while finer anatomical details such as grooves and ridges were smoothed out.

To represent the internal tissue structure of the auricle, a hollow auricle model with a thin 1 mm shell thickness was first generated. This generated inner volume was extracted. The lobule part of the extracted part was truncated to form the cartilage section. The skin layer was generated by subtracting the cartilage section from the original model.

To manufacture the phantom from the CAD model, a combination of soft material 3D printing and silicone rubber moulding was used. The shape of the mould box was defined in CAD by subtracting the auricle model from a cuboid. This mould shape was then separated into three pieces. Figure 3(b) shows the assembly of the corresponding mesh files. The spatial axes of the auricle phantom are defined by three axes: superior to inferior, anterior to posterior, and lateral left to right.

Figure 3(c) illustrates the manufacturing process used for the two-layer phantom auricle model. Three different materials were used in this process. The cartilage was first printed with a 3D printer (Form 3B; Formlabs, US) with a soft and elastic material (Elastic 50A Resin; Formlabs, US) with a Young's modulus of 3.35 MPa. Then, the same printer produced the three-piece transparent mould box for the phantom model, employing a clear and stiff material (Clear Resin V4; Formlabs, US). This transparency allowed for observing and controlling the injection of silicone rubber into the mould.

Finally a silicone rubber (silastic 3481; ECF Composite Ltd., UK) with a Young's modulus of 0.42 MPa was prepared and injected into the empty space of the mould box, enveloping the pre-inserted cartilage part, thus creating the two-layer phantom model. The Young's moduli of the materials detailed above were measured using dog-bone-shaped specimens in a tensile test (see supplementary material 1).

The cartilage part and the resulting two-part phantom model are illustrated in Figure 3(d).

2.2. Application of Phantom to Develop Auricle Mechanical Test Methods

In this section, we illustrate the utility of the phantom to characterise auricle mechanical behaviour, using it to develop test methods to measure the structural response of the auricle. These are applied, slightly modified, to the human volunteer studies of section 3. These human auricle results will also be used to confirm that the phantom behaves in a realistic manner.

Two mechanical tests were developed: a static loading test to measure the structural deformation of the auricle under static loading and a dynamic loading test to measure the natural frequency of the auricle structure and analyse its vibration response.

2.2.1. Static loading test

In the static loading test, an Instron universal testing machine (Instron 3384; Illinois Tool Works, Inc., US) applied a load to a clip attached to the tip of the auricle phantom via a cotton thread (Figure 4a). A 10 N capacity load cell measured the applied load. The clip was marked with green to clearly indicate the pulling point (P). This point of attachment was the tubercle of the auricle, which is on the posterior tip of the helix. The test was video recorded with a Pixelink camera (Pixelink, CA) and the images were processed

using bespoke MATLAB code (MATLAB 2022a; The Mathworks Inc., US) to calculate the displacement of P. This straightforward pulling of the ear provides the variation of force with displacement resulting from the deformation of the external ear.

Two loading variants were tested: lateral loading (pulling outward from the skull to the body midplane) and anterior loading (applying force from the back to the front of the body). With lateral loading, the auricle bent initially, followed by significant stretching. Anterior loading primarily caused bending with minimal stretching. Displacements of the clip point along the pulling axis were calculated, as illustrated in Figure 4(d) and (e). The anterior loading required less force to achieve the same deformation as lateral loading, making it a more suitable and comfortable protocol for human auricle testing.

This testing protocol was developed to provide a simple structural test which could be applied to volunteers. However, the load set-up meant that the specific trajectory at the load point depended on the details of the auricle geometry and deformation. While it would have been possible to apply a defined trajectory at the load point with a rigid loading link, this would have been more challenging to implement for the human volunteers, especially with dynamic loading. The remote prescribed trajectory, with loading through the thread, provided a trade-off between a well-defined deformation trajectory and one which was feasible on volunteers.

2.2.2. Dynamic Loading Test

A dynamic loading test is necessary to characterise the mechanical response of the auricle during movements, including the determination of natural frequency and damping characteristics of the auricle. The dynamic response of the auricle-earable system is expected to be an important part of earable design.

The dynamic loading test first involved applying a load statically, in the same way as described in the previous section. The load was then released suddenly by burning the loading thread, allowing the auricle to oscillate back to its original shape. The experimental set-up is illustrated in Figure 5(a). This test is based on step loading release techniques commonly used for investigating natural frequencies in other structures (Fu and Song, 2020).

Markers were painted on the auricle phantom, and a video of its deformation was recorded. This video was processed with MATLAB code to track marker displacement. Figure 5(b) and (c) show the anterior and superior views of the phantom vibration, including superimposed coloured markers tracking the trajectory of the deformation. The displacement of these markers in the lateral direction, relative to the location at rest, is plotted as a function of time for each of the three points in Figure 5(d) and (e).

The location of the marker position $y(t)$ as a function of time t can be fitted with a MATLAB script as

a damped sinusoidal function:

$$y(t) = A^{-\lambda t} cos(2\pi f t - \varphi) \tag{1}$$

where A is the amplitude of the motion, λ is a decay coefficient, $\tau = 1/\lambda$ is the damping time constant, f is the natural frequency of the movement in Hz, and φ is a phase shift. This study aims to characterise the natural frequency and damping properties of the auricle, which are represented by f and τ. Figure 5(f) shows the results of fitting the cyan point trajectory in Figure 5(d), with in this case a resulting estimated natural frequency $f = 49.1$ Hz and decay coefficient $\lambda = 48.67$ s^{-1}, which indicates τ for the phantom is 21 ms.

The calculated natural frequency f and damping time constant τ of the auricle model are key parameters to validate the dynamic model of the real ear and are needed for analysing how different ear geometries and material properties can affect the mechanical properties of the ear.

In summary, this section has described details of the design and manufacturing methodology to construct a realistic auricle phantom to investigate the mechanical response of the ear. The phantom has been used to develop a test protocol to be applied in the next section to human volunteers. Both the test set-up and analysis procedure have been optimised for application to human subjects, illustrating the utility of the phantom.

3. Characterisation of Human Auricle Structural Properties from a Volunteer Study

The test methods developed for the auricle phantom model, as detailed in the previous section, effectively measured the static and dynamic responses of the phantom. Due to the auricle's structural complexity and variability across individuals, directly measuring material properties to evaluate the auricle mechanical behaviour is challenging. Instead, these tests provide a structural perspective on auricle mechanics. Building on this approach, the methods were adapted for a human volunteer study with the aim of characterising experimentally the structural response of the human auricle.

3.1. Volunteer Study Methods

3.1.1. Experimental Set-up

Figure 6 shows the set-up for the human volunteer experiment. Participants were seated with their heads stabilized on a chin rest to ensure consistent positioning during the experiment. The auricle loading protocol followed closely that developed with the phantom auricle. An ear clip was attached to the participant's auricle at the tubercle and connected to a thread extending to the anterior of the auricle, aligned with the

axis measuring the ear's width. This setup ensured a controlled bending motion for the experiment. A static anterior pull was applied to the thread, followed by a dynamic release through burning the thread, allowing for the recording of the resulting oscillations.

The thread was connected to a pulley system driven by a stepper motor (model MFA-PPD; Newport Spectra-Physics Ltd., US) with a maximum displacement of 25 mm. A load cell (GSMTM-4.5N; Interface, Inc., US), with a measurement range of 4.5 N, was attached at the stepper-motor end of the string to measure the applied force on the string. To record the deformation of the auricle, a Sony ZV-1 camera (Sony Europe BV, UK) was connected to the test system, synchronously capturing the auricle deformation as the motor started pulling. Photometric markers, which were blue dots painted on white medical tape, were applied to the auricle of the test subject to track deformation.

Test subjects ranged from 18-40 years old, comprising 8 male and 7 female participants. The volunteer study was approved by the Research Ethics Committee of the Department of Engineering, Cambridge, and all participating subjects provided written, informed consent for this study.

3.1.2. Data Collection

The auricle length and width of the test subjects were measured from the captured auricle images. These images included a reference scale, positioned in the same plane as the auricle to ensure that the measurements are not distorted by perspective or depth differences. The length of the auricle was defined as the greatest diameter on the auricle. This would typically be from the top to the bottom of the auricle. The width was defined and measured as the longest distance across the auricle, taken perpendicular to the length measurement.

The experiment started with the static test, where the stepper motor pulled the string in the anterior direction at a speed of 0.5 mm s^{-1}. The pulling process lasted for the 25 mm range of the stepper motor. The deformation process was recorded with a series of photographs taken every second. The force readings from the load cell and the displacement of the stepper motor were also recorded. A MATLAB script tracked the displacement of the auricle markers.

For the dynamic test, the starting condition was the end of the static test. The string connecting the clip to the stepper motor was then burnt. The subsequent oscillatory motion was captured by the camera's high-frame mode at 1000 frames per second (fps). The same MATLAB script analysed the auricle's deformation, extracting the displacement of markers over time from the recorded video. Subsequent data processing and statistical analysis were performed with MATLAB. A confidence level of 0.05 was used to test for statistical significance.

3.2. Volunteer Study Results

This section provides the results of the human auricle volunteer study. The section starts by describing the measurements of the auricles and then presents results for the static and dynamic tests, using the analysis protocols described from the phantom methodological development study of section 2.

3.2.1. Auricle Dimensions

Figure 7(a) plots the range of auricle lengths and widths measured for all the test subjects. To determine whether there were significant differences between males and females, t-tests were conducted on both width and length measurements. The null hypothesis was that there was no difference in auricle width or length between male and female groups. Results showed that male and female auricles differed in both length and width at a 0.05 confidence level, as detailed in Table 2.

3.2.2. Static Test Results

The static test aimed to characterise the stiffness of the human auricle structure due to static loading. To compare the displacements of auricles with different dimension, the distance travelled by the clip in the anterior direction of the ear was normalised by dividing by the auricle width w. The results of the static load tests are plotted in Figure 7(b) for all 15 participants, showing the applied force as a function of the normalised displacement.

To further compare results across participants, a standardised load was defined as the force required in the static load test to reach a normalised displacement of 0.25. Table 2 includes this analysis. The average value of this standard load for the 15 test subjects was 117 mN, with a standard deviation (SD) of 17 mN. There was no significant difference in this standard load between the male and female test groups.

3.2.3. Dynamic Test Results

The dynamic tests aimed to characterise the dynamic response of the human auricle, and in particular to measure the natural vibration frequency and damping properties of the auricle. As detailed in Table 2, the average value of the natural frequency(f) for the 15 test subjects was 20.6 Hz, with a standard deviation of 3.7 Hz. The average value of the damping constant (τ) was 29.3 ms, with a standard deviation of 8.0 ms. T-tests indicated no significant difference in natural frequency between males and females; however, the damping time constant showed a statistically significant difference, as detailed in Table 2.

Figures 7(c) and (d) present further details of the dynamic test results, showing the regression of natural frequencies plotted against auricle length and width. First-order linear regression was performed for both

auricle dimensions against the natural frequency f of the auricle, with the line of best fit and its 0.05 confidence intervals plotted. The natural frequency was inversely correlated with both the auricle length and width, albeit with modest R^2 regression coefficients of -0.37 and -0.49, respectively.

In summary, this study provides the first detailed characterization of the structural mechanical response of the human auricle, analysing auricle size, as well as its static and dynamic behaviour, in 15 volunteer subjects.

4. Development of a Finite Element Model of Auricle Mechanical Behaviour

This section outlines the development of an FE model of the auricle. The aim is to provide a tool to simulate the mechanical and structural response of the auricle, with a focus on helping design and optimise earables. An FE model was first developed for the phantom to check that the approach was accurate for this well-defined test case. The same approach was then applied with human auricle material properties and results compared with the human volunteer study to validate the model.

4.1. FE Model of Phantom Auricle

4.1.1. Phantom FE Model Methodology

To generate the auricle phantom model, the same auricle model used in the phantom construction was further meshed at varying mesh densities using MeshLab (Cignoni et al., 2008) and then imported into Abaqus 2018 (Dassault Systèmes, FR) for FE analysis. Second-order tetrahedral elements (C3D10) were used, as they are commonly employed in 3D biomechanical models due to their ease of automatic generation and good performance under large deformations.

A mesh convergence test was performed to determine the optimal mesh density, balancing computational efficiency and accuracy (Bright and Rayfield, 2011). This involved evaluating meshes with different densities and evaluating the resulting changes in key mechanical outputs. Based on the test results, elements with an average seed length of 1.0 mm were chosen as appropriately accurate, ensuring that further refinement did not lead to significant changes in the simulation outcomes (see Supplementary Material 2 for details).

The FE model for the phantom included separate parts representing the skin and cartilage. These were both modelled as linear elastic materials, using the measured elastic modulus values as detailed in Table 1. The Poisson's ratio for both materials was assumed to be 0.48 as suggested in other FE studies on rubber and silicone gel materials(Imam et al., 2023).

The phantom exhibited significant damping in the dynamic tests. This time-dependent behaviour is presumably associated with the visco-elastic nature of the materials used in the phantom. This behaviour is also considered to be an important part of the human auricle mechanical performance, as it will significantly affect the performance of earables mounted on the auricle. One approach to modelling this time-dependent material behaviour would have been to use a visco-elastic material formulation. However, to simplify the model and given the lack of data on visco-elastic material properties of the auricle, we instead adopted a pragmatic approach, commonly used in structural modelling, of using Rayleigh damping. This is implemented in Abaqus using the *DAMPING option. The Rayleigh damping parameters α and β for mass and stiffness proportional damping, respectively, were taken as $\alpha = 0\ s^{-1}$, $\beta = 1 \times 10^{-3}\ s$ (Gan et al., 2004). Hence only the stiffness-proportional term associated with material damping was included.

The load cases and boundary conditions were specified to model the static and dynamic load cases described in the previous sections. The assumption was made that the model incorporates non-linear geometric FE modelling (i.e., large displacement modelling). Details of the applied boundary conditions and assembly setup are included in Supplementary Material 2.

4.1.2. Phantom FE Model Results

Figure 8(a) compares the simulation and experimental results of the static load test, for anterior loading on the phantom model. Agreement is good.

The results from the dynamic simulation are shown in Figure 8(b), plotting the anterior displacement of the loading point on the auricle as a function of time. This can be compared with the experimental results plotted in Figure 5. Again there is excellent agreement in the response, with the measured natural frequency of 49.1 Hz comparing well with the estimated natural frequency from the computational model of 48.1 Hz.

In summary, the FE model has a static and dynamic mechanical response in good agreement with the measured response of the phantom. This confirms the effectiveness of the modelling approach for this well-defined case where the geometric and elastic properties of the model conform to the experimental setup.

4.2. FE Model of Human Auricle

Having demonstrated the effectiveness of the FE approach for the phantom, we now follow a similar approach using material properties appropriate to the human auricle, comparing the results with the volunteer test results to validate the model.

4.2.1. Human Auricle FE Model Methodology

Figure 9(a) presents the human auricle model, with the top half rendered transparent to reveal the thin cartilage layer cavity at its core. This model is directly remeshed from the original segmented auricle without any simplification, preserving all anatomical features. In contrast, the phantom auricle has a greater thickness than the human auricle model, allowing it to be more practical for construction.

In this simulation, a linear elastic material model is employed for both components of the auricle with a Poisson's ratio of 0.48 (Oatis, 2013). The material moduli were adopted from literature values, as detailed in Table 1, to effectively capture the elastic response under small deformations. However, for future studies, this linear model will be replaced with a hyperelastic model. A detailed investigation into the hyperelastic properties of auricle skin and cartilage will be undertaken, with the aim of refining FE simulation results and enhancing comparisons with volunteer test outcomes.

The same boundary conditions and assembly were used for the realistic model as for the phantom model except the Rayleigh Damping constant β is halved to 5×10^{-4} s.

4.2.2. Human Auricle FE Model Results

Results from the static and dynamic loading simulations for the human auricle model are presented in Figures 9(b) and (c), respectively. For static loading, the simulated force at a normalised displacement of 0.25 (normalised by the auricle width) is 120 mN (see Fig. 9(b)), which is very close to the mean measured value of 117 nM from the volunteer study as reported in Table 2. The predicted natural frequency of the realistic model is 21.6 Hz, which again closely matches the mean natural frequency of the volunteer study of 20.6 Hz. The value of the decay coefficent λ derived from the fitted function (equation 1) is 28.3 s^{-1}. The corresponding damping time constant is $\tau = 1/\lambda = 35.3$ ms, within one standard deviation of the mean value of 29.3 ms measured for the volunteer group.

In summary, an FE model of the human auricle has been developed which can model the static and dynamic response of the auricle, and so provides a useful tool for designing and optimising earables. The model has been validated by comparison with experimental results taken from the volunteer study, showing good agreement both in the static and dynamic response. Further validation through additional datasets and simulations will enhance the accuracy and predictive capabilities of the computational model.

5. Discussion

In this paper, we developed a phantom auricle model which can be used to investigate experimentally the mechanical response of auricles. The model's low cost and ease of manufacture make it a valuable tool for a variety of studies. However, modifications can be made to bring its mechanical properties more in line with the volunteer study measurements. For instance, reducing the material stiffness and adjusting the wall thickness to better mimic the human auricle are expected to lower both the overall stiffness and natural frequency of the model. Further adjustment to the materials and dimensions of the auricle model could help the phantom represent a diverse population. Advanced 3D printing technology could be used to enable manufacturing with materials of different stiffnesses to print a realistic auricle (Iftekar et al., 2023).

The mechanical experiment conducted on volunteers successfully measured the structural response of the human auricle to external forces. Characterizing these properties for the first time provides valuable data on the auricle's response in static or dynamic scenarios involving more complex loading. For instance, the findings offer insights into how vibration is transmitted to earable devices during daily activities such as walking and running.

The static response was measured by loading the auricle tip anteriorly and measuring the resulting tip deformation. The auricle stiffness was compared with the loads corresponding to a normalised displacement equal to 25% of the auricle width. This load was surprisingly uniform between participants, having a standard deviation of 15% of the mean value 117 mN. The auricle stiffness showed no statistical difference between gender groups and showed only a weak correlation with auricle dimensions. Additional structural tests, such as using a load clip with accelerometer attached human auricle under different motion, could provide deeper insights into mechanical properties of the auricle and provide further guidelines to earable design.

The dynamic properties were measured using load-release tests. Analysis was used to extract the natural frequency f and damping time constant τ. There was a significant difference in τ between the male and female groups, but no difference was seen in the natural frequency between genders.

A computational model for the mechanical behaviour of the auricle was developed, allowing future investigation of its response under varying conditions. The two-component model effectively recreated a human auricle. Results of both static and dynamic simulations agreed well with measured values from the phantom and volunteer studies. A linear elastic material model was used. This would be expected to lose accuracy for high strains (e.g. above 20%), when a hyper-elastic material model would be more appropriate. However, it is likely that the applicable range of deformations is less than those tested in this study, which

were rather extreme cases used to provide clearer measurements particularly of the dynamic response. The visco-elastic material behaviour was modelled using Rayleigh stiffness-proportional damping. Although this was found to capture the damping behaviour of the phantom and human auricles effectively, more detailed studies on time-dependent structural properties would warrant including a visco-elastic material formulation.

Future studies will aim to generalise a model for auricle structural properties by using computational simulations with key parameters to estimate the full mechanical properties of human auricles based on limited measurements. Future work could focus on generating auricle models that represent a wider range of the population. Using statistical algorithms, various auricle models can be generated that incorporate different mechanical properties (Reed and Bonifas, 2023). The load case chosen for the tests and simulation, anteriorly pulling the tubercle of the ear via a clip and thread provided a reasonable well-defined test case which could be implemented in a volunteer study. The FE model could be used to investigate a wider range of load cases, additionally including the effect of an earable on the dynamic response.

6. Conclusions

This study aimed to provide tools and characterisation data to allow assessment of the mechanical behaviour of the human auricle, especially as related to earable design and use.

The 3D printing and moulding process described in the paper can be used to make a realistic two-component physical auricle phantom which serves as a valuable experimental tool for modelling auricle dynamics. Its worth has been demonstrated in developing a testing methodology for the human auricle volunteer study.

Experimental data measuring the human auricle static and dynamic response have been collected from volunteer subjects. For the first time this provides key characterisation metrics which can be used to describe the auricle mechanical response. Natural frequencies ranged from 14 to 28 Hz, while loads for a standardised auricle deflection varied between 91 and 143 mN. Significant variations in auricle dimensions were observed, with males having statistically larger auricles than females.

Finite element models for the phantom and human auricles have been developed based on CT geometry data with a two-component structure and linear elastic material models. These were found to predict static and dynamic responses in good agreement with the phantom and human auricle measurements, validating the overall approach. These models can be adapted to model a diverse population and can be used to simulate the mechanical response to a range of load cases.

In summary, the tools and characterisation data presented in this paper can be used in simulations of

proposed earable designs to understand the interaction between auricle properties, earable design and their impact on mechanical response and performance.

Acknowledgements

We are grateful to the W.D Armstrong Trust for the funding of YL. We are also most grateful to all the volunteers who participated in the study. We would like to express our appreciation to S.R. Marshall, G. Smith, and S. Savage (Department of Engineering, University of Cambridge, Cambridge, United Kingdom) for their invaluable assistance and support throughout the experimental process.

References

Areias, B., Parente, M., Gentil, F., Santos, C., Natal Jorge, R., 2017. A numerical study of the human ear, in: 2017 IEEE 5th Portuguese Meeting on Bioengineering (ENBENG), pp. 1–4. doi:10.1109/ENBENG.2017.7889442.

Baker, S.R., 2021. Local flaps in facial reconstruction / Shan R. Baker. Fourth edition. ed., Philadelphia : Saunders.

Benacchio, S., Doutres, O., Le Troter, A., Varoquaux, A., Wagnac, E., Callot, V., Sgard, F., 2018. Estimation of the ear canal displacement field due to in-ear device insertion using a registration method on a human-like artificial ear. Hearing Research 365, 16–27.

Brenner, S.C., Scott, L.R., 2008. The Mathematical Theory of Finite Element Methods. volume 15 of *Texts in Applied Mathematics*. Springer.

Bright, J.A., Rayfield, E.J., 2011. The response of cranial biomechanical finite element models to variations in mesh density. The Anatomical Record 294, 610–620.

Cardoso, L., Cowin, S., 2012. Role of structural anisotropy of biological tissues in poroelastic wave propagation. Mechanics of materials : an international journal 44, 174–188. doi:10.1016/j.mechmat.2011.08.007.

Choudhury, R.R., 2021. Earable computing: A new area to think about, in: Proceedings of the 22nd International Workshop on Mobile Computing Systems and Applications, Association for Computing Machinery, New York, NY, USA. p. 147–153.

Cignoni, P., Callieri, M., Corsini, M., Dellepiane, M., Ganovelli, F., Ranzuglia, G., 2008. MeshLab: an Open-Source Mesh Processing Tool, in: Scarano, V., Chiara, R.D., Erra, U. (Eds.), Eurographics Italian Chapter Conference, The Eurographics Association. doi:10.2312/LocalChapterEvents/ItalChap/ItalianChapConf2008/129-136.

Debener, S., Emkes, R., De Vos, M., Bleichner, M., 2015. Unobtrusive ambulatory EEG using a smartphone and flexible printed electrodes around the ear. Sci Rep 5, 16743.

Felfela, G.M.W., 2017. Ear anatomy. Egypt: Juniper Publishers .

Fu, L., Song, A., 2020. Model-based load characteristics analysis of the multi-dimensional force sensor. IEEE Access 8, 116431–116440. doi:10.1109/ACCESS.2020.3004113.

Gan, R., Feng, B., Sun, Q., 2004. Three-dimensional finite element modeling of human ear for sound transmission. Annals of biomedical engineering 32, 847–59. doi:10.1023/B:ABME.0000030260.22737.53.

Goyal, K., Borkholder, D.A., Day, S.W., 2022. Dependence of skin-electrode contact impedance on material and skin hydration. Sensors 22.

Griffin, M., Premakumar, Y., Seifalian, A., Szarko, M., Butler, P., 2016. Biomechanical characterisation of the human auricular cartilages; implications for tissue engineering. Annals of Biomedical Engineering 44.

He, D.D., Winokur, E.S., Sodini, C.G., 2015. An ear-worn vital signs monitor. IEEE Transactions on Biomedical Engineering 62, 2547–2552.

Hendriks, F., Brokken, D., van Eemeren, J., Oomens, C., Baaijens, F., Horsten, J., 2003. A numerical-experimental method to characterize the non-linear behaviour of human skin. Skin research and technology : official journal of International Society for Bioengineering and the Skin (ISBS) [and] International Society for Digital Imaging of Skin (ISDIS) [and] International Society for Skin Imaging (ISSI) 9, 274–83.

Higgins, M., Leung, S., Radacsi, N., 2022. 3d printing surgical phantoms and their role in the visualization of medical procedures. Annals of 3D Printed Medicine 6, 100057.

Homicz, M., McGowan, K., Lottman, L., Beh, G., Sah, R., Watson, D., 2003. A compositional analysis of human nasal septal cartilage. Archives of facial plastic surgery 5, 53–8. doi:10.1001/archfaci.5.1.53.

Hrncirik, F., Roberts, I.V., Swords, C., Christopher, P.J., Chhabu, A., Gee, A.H., Bance, M.L., 2022. Impact of scala tympani geometry on insertion forces during implantation. Biosensors 12.

Iftekar, S.F., Aabid, A., Amir, A., Baig, M., 2023. Advancements and limitations in 3d printing materials and technologies: A critical review. Polymers 15, 2519.

Imam, S., Hughes, A., Carré, M., Driscoll, H., Winwood, K., Venkatraman, P., Allen, T., 2023. Finite element model to simulate impact on a soft tissue simulant. Sports Engineering 26. doi:10.1007/s12283-023-00407-7.

Kappel, S.L., Rank, M.L., Toft, H.O., Andersen, M., Kidmose, P., 2019. Dry-contact electrode ear-eeg. IEEE Transactions on Biomedical Engineering 66, 150–158.

Oatis, C., 2013. Kinesiology: The mechanics and pathomechanics of human movement: Second edition. Lippincott Williams & Wilkins. chapter 5. pp. 1–946.

Papapanagiotou, V., Diou, C., Zhou, L., van den Boer, J., Mars, M., Delopoulos, A., 2017. The splendid chewing detection challenge, in: 2017 39th Annual International Conference of the IEEE Engineering in Medicine and Biology Society (EMBC), pp. 817–820.

Pawlaczyk, M., Lelonkiewicz, M., Wieczorowski, M., 2013. Age-dependent biomechanical properties of the skin. Postepy dermatologii i alergologii 30, 302–306.

Reed, M.P., Bonifas, A., 2023. Development of a Parametric Model of Adult Human Ear Geometry. Technical Report. UMTRI.

Röddiger, T., Clarke, C., Breitling, P., Schneegans, T., Zhao, H., Gellersen, H., Beigl, M., 2022. Sensing with earables: A systematic literature review and taxonomy of phenomena. Proc. ACM Interact. Mob. Wearable Ubiquitous Technol. 6.

Wu, H., Yang, G., Zhu, K., Liu, S., Guo, W., Jiang, Z., Li, Z., 2021. Materials, devices, and systems of on-skin electrodes for electrophysiological monitoring and human-machine interfaces. Advanced Science 8, 2001938.

7. Figures

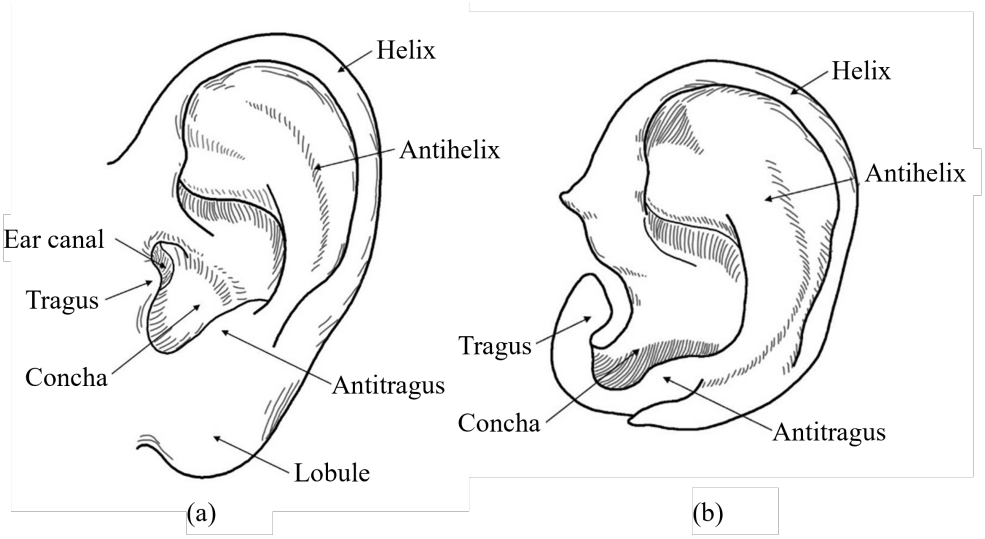


Figure 1: Anatomical Structure of (a) auricle and (b) auricle cartilage. Illustrations were adapted from (Baker, 2021)
.

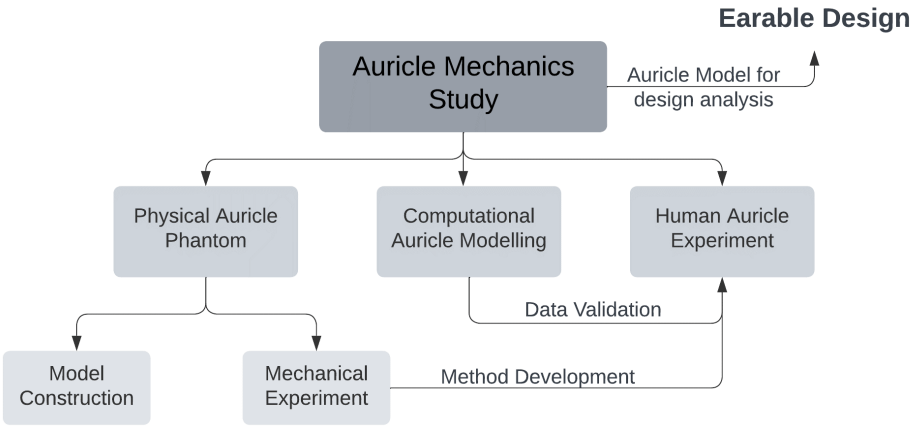


Figure 2: Project roadmap for modelling human auricles

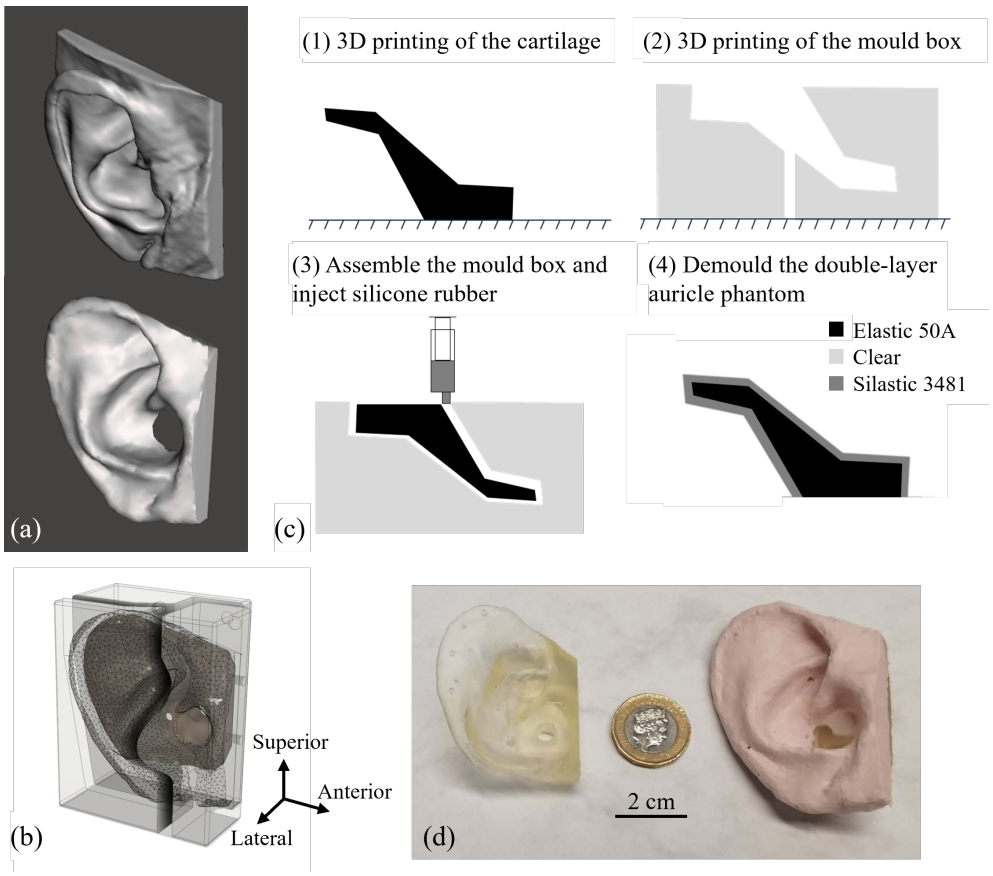


Figure 3: Phantom model construction: (a) Segmented and simplified ear model. (b) Assembled mould box and cartilage layer, with the anatomical directions relative to the auricle defined. (c) Manufacturing steps for the phantom auricle model. Cartilage section is 3D printed with Elastic 50A resin. Mould box is also printed with clear resin. Skin is made of the injected silicone rubber silastic 3481. (d) Manufactured auricle phantom, left is the 3D printed cartilage, right is the final phantom.

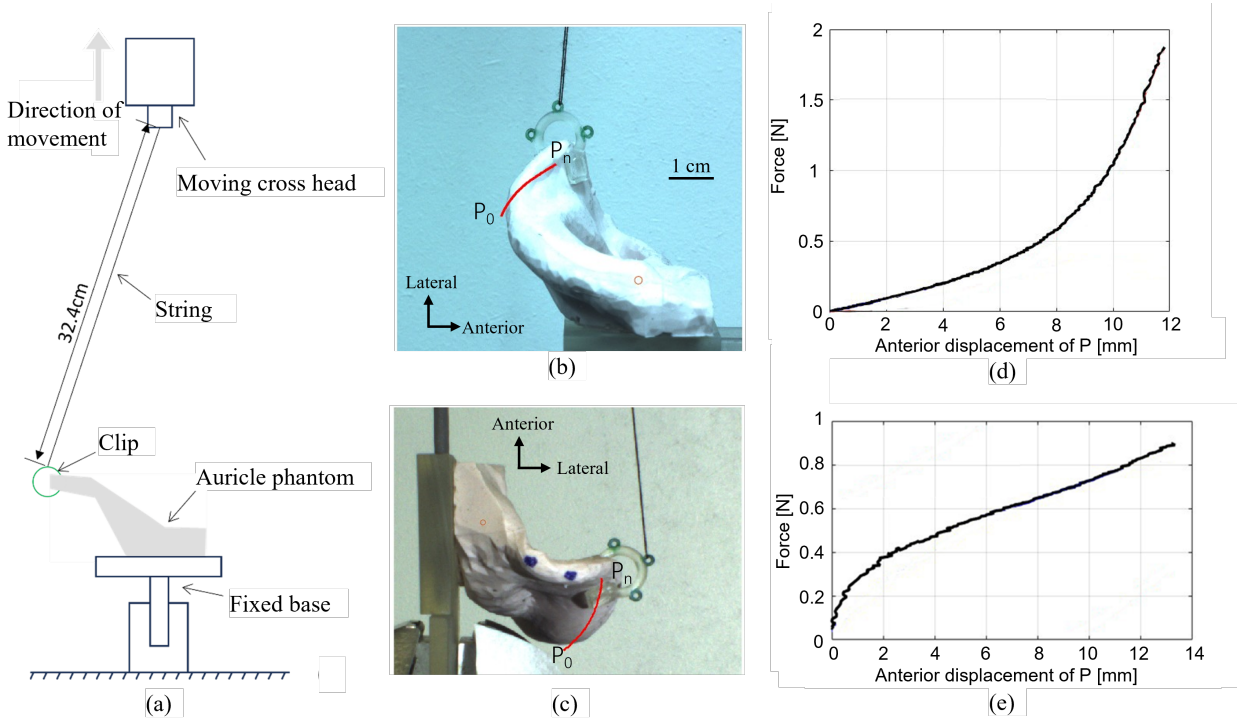


Figure 4: (a) Schematic of the static experiment set-up for the auricle phantom from an inferior view. The applied load direction is either: (b) lateral pulling from an inferior view or (c) anterior pulling from inferior view. The anterior distance travelled by the clip point P as a function of the applied load is given for: (d) lateral loading and (d) anterior loading.

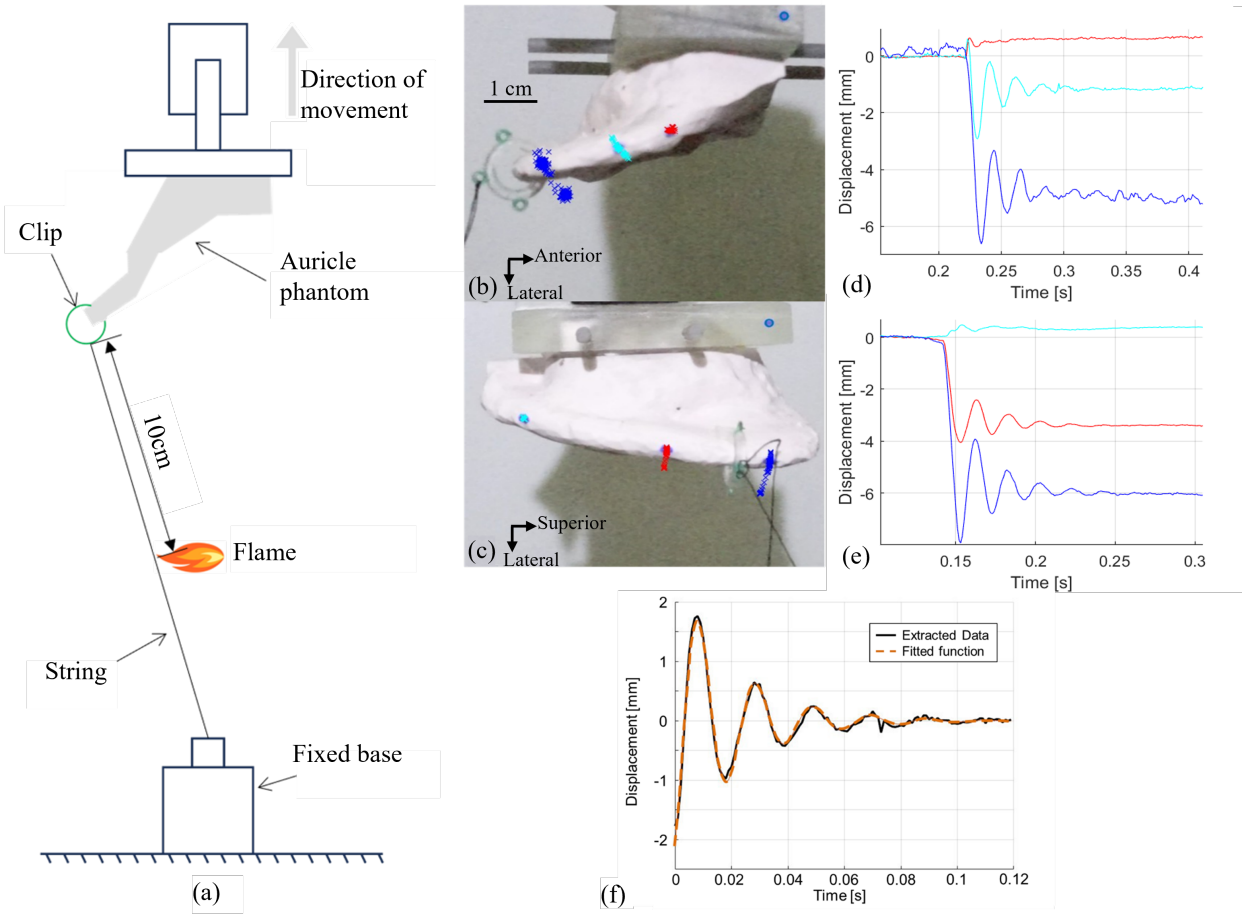


Figure 5: (a) Schematic of the dynamic experiment set-up. Frames from the video capture the dynamic experiment seen from (b) a superior view and (c) a posterior view. The displacements of the three markers in the lateral direction are plotted as a function of time from (d) a superior view and (e) a posterior view. Each coloured line corresponds to the marker with the same colour. (f) Displacement of the blue marker in figure 5 with a negative initial displacement. The fitted damped oscillation is also plotted in orange dashed line. The calculated natural frequency is 49.1 Hz for the phantom auricle model.

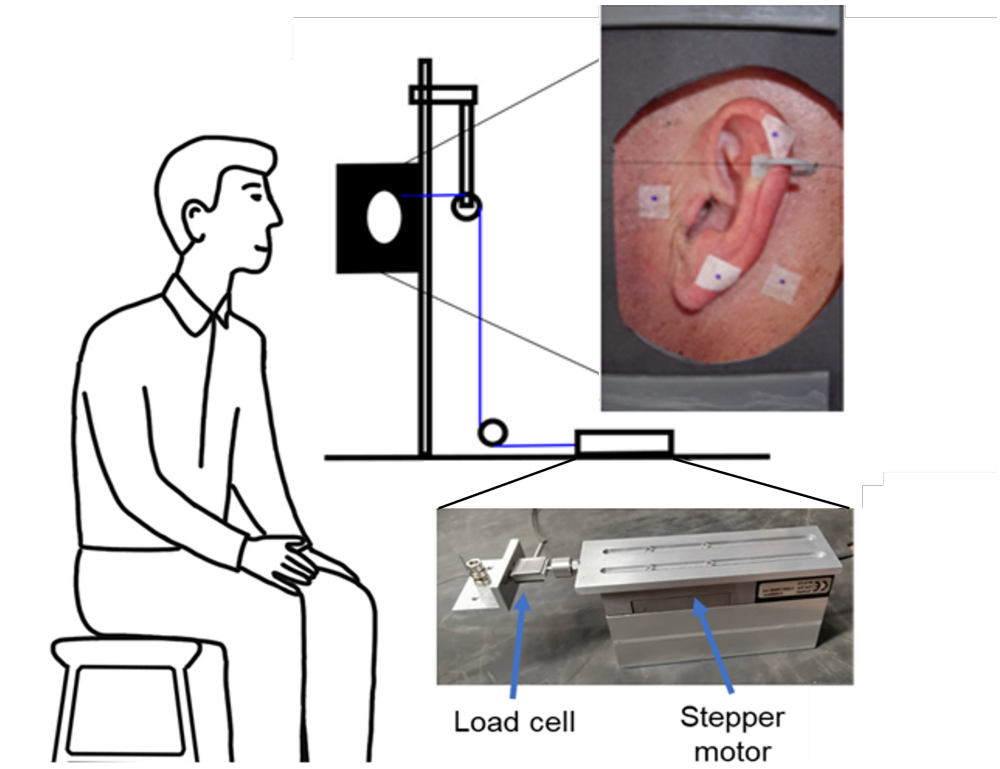


Figure 6: Volunteer experimental set-up. The test subject's head is rested on a chin rest. The ear is taped with markers and shielded with a black background. The stepper motor moves to deform the auricle and the load cell measures the force applied.

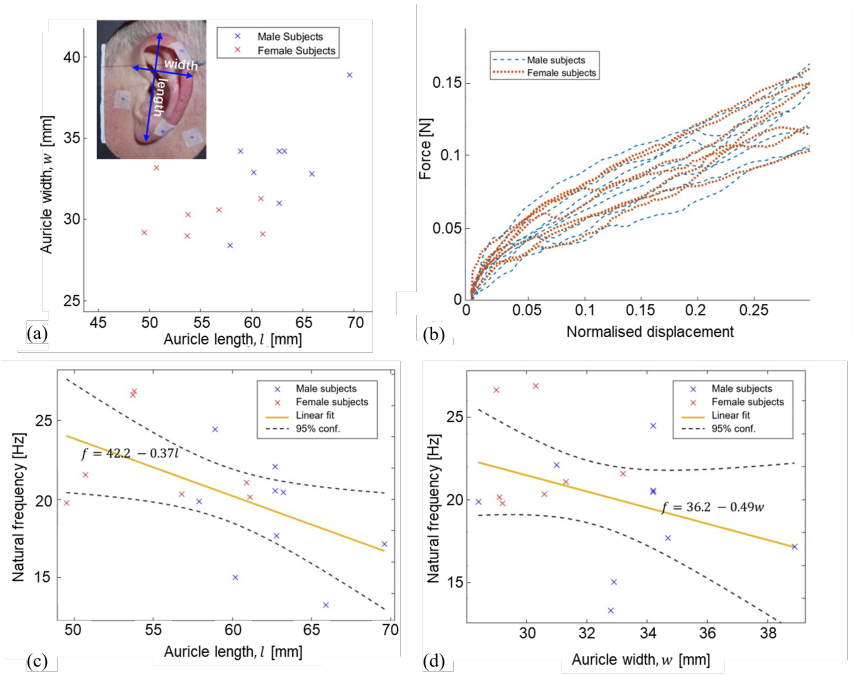


Figure 7: Results of auricle volunteer study. (a) Auricle dimensions of test subjects. (b) Static test response plotting the change in the anterior displacement, normalised by the auricle width, for loading in the anterior direction. (c) & (d) Calculated natural frequency from dynamic tests of the auricle as a function of (c) auricle length and (d) auricle width. First order line of best fit with 0.05 confidence intervals for the coefficient range are plotted as dashed line regions in (c) and (d).

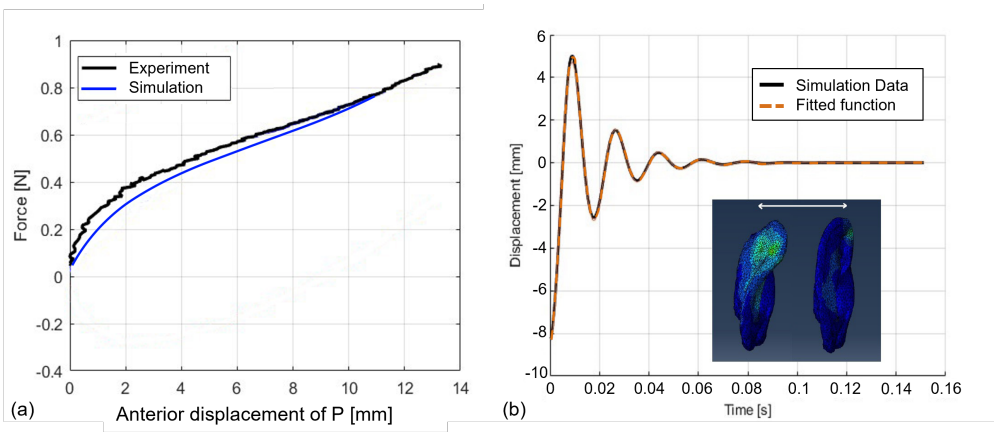


Figure 8: Results of the phantom FE study. (a) Comparison of the static response from the simulation with the experimental response, showing the applied force as a function of displacement. (b) Simulation results for dynamic lateral displacement plotted as a function of time. The fitted damped oscillation is shown with an orange dashed line, corresponding to a calculated natural frequency of 48.7 Hz. For reference, the natural frequency of the phantom model is 49.1 Hz, as shown in Figure 5.

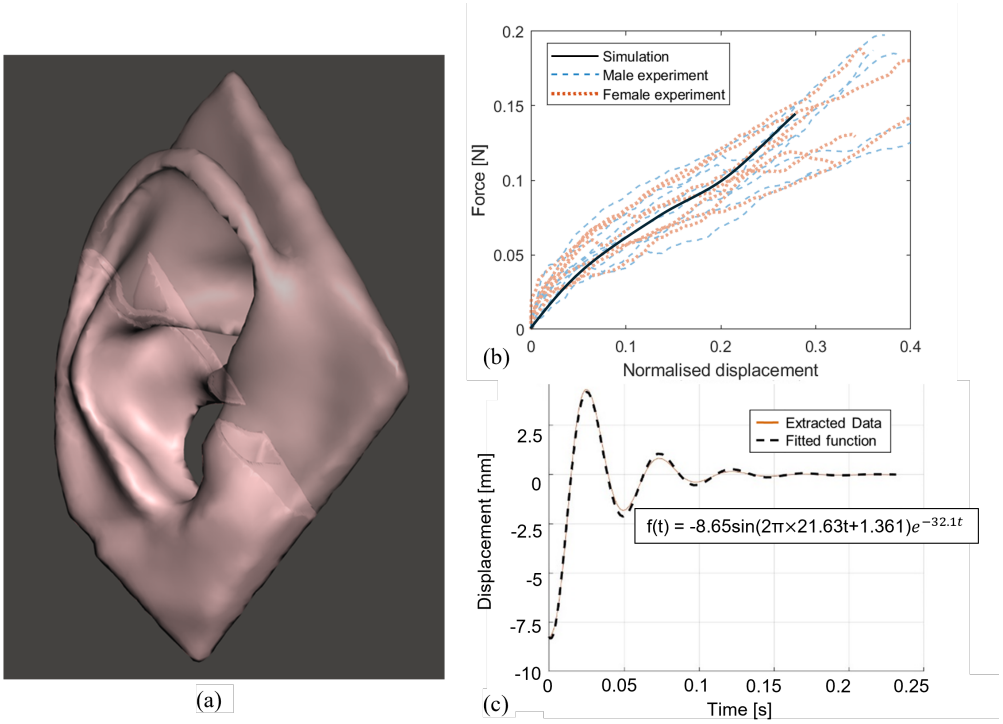


Figure 9: Results of the human auricle FE study. (a) Illustration of the human auricle FE model. The top half of the model is shown as transparent to reveal the cartilage layer inside. (b) The static response from the simulation with normalised displacement - the loading point displacement normalised by the auricle width w - plotted against the applied force. Volunteer experiment results are plotted for direct comparison; (c) Dynamics response from the simulation. The lateral displacement of a point on the auricle tip is extracted and plotted as a function of time. The function is then fitted with the damped oscillation function, showing the natural frequency of the computational model is 21.6 Hz.

8. Tables

Material property	Auricle phantom model	Human auricle model
Cartilage Density	1.01×10^3 kg m^{-3}	1.1×10^3 kg m^{-3}(Homicz et al., 2003)
Skin Density	1.15×10^3 kg m^{-3}	1.09×10^3 kg m^{-3}(Cardoso and Cowin, 2012)
Cartilage Young's modulus	3.35 MPa	1.05 MPa (Griffin et al., 2016)
Skin Young's modulus	0.42 MPa	0.15 MPa (Hendriks et al., 2003)
Poisson's ratio	0.48 (Imam et al., 2023)	0.48 (Oatis, 2013)

Table 1: Material properties assigned in the FE simulations to the phantom and realistic human models. The density of the phantom model materials are provided in the material datasheets. The moduli for the phantom model were measured directly by the authors (see supplementary material 2), while the properties of the human auricle model and Poisson's ratios were based on literature sources as indicated in the table.

Parameters	Subject group	N	Mean	SD	t-statistics
Length [mm]	All	15	59.2	5.6	p = 0.0046
	Male	8	62.6	3.8	
	Female	7	55.2	4.6	
Width [mm]	All	15	31.9	2.8	p = 0.036
	Male	8	33.3	3.0	
	Female	7	30.4	1.5	
Standard load [mN]	All	15	117	17	p = 0.61
	Male	8	115	17	
	Female	7	120	18	
Natural frequency (f) [Hz]	All	15	20.6	3.7	p = 0.092
	Male	8	19.1	3.7	
	Female	7	22.4	3.1	
Damping constant (τ) [ms]	All	15	29.3	8.0	p = 0.039
	Male	8	33.2	8.0	
	Female	7	24.9	5.2	

Table 2: Volunteer test result statistics. Statistical analysis of volunteer test results included t-tests on all measured parameters, with the null hypothesis stating that there is no difference between male and female groups. At a 0.05 confidence level, significant differences were found between the male and female groups in terms of auricle width, length, and damping constant.